INFLUENCE OF OPERATING CONDITIONS UPON THE DYNAMIC STEADY-STATE PERFORMANCE OF A SWITCHED RELUCTANCE MOTOR

J. Faiz

Department of Electrical and Computer Engineering
Faculty of Engineering
University of Tehran
Tehran, Iran

E. Shafagh

Department of Electrical Engineering
Faculty of Engineering
University of Tabriz
Tehran, Iran

(Received: Oct. 1, 1998 - Accepted in Revised form: April 8, 1999)

Abstract In order to obtain more accurate predicted dynamic steady-state performance with shorter computation time, an available mathematical model is modified and presented. Using this modified model, performance of a typical switched reluctance motor (SRM) under a wide range of variations of operating conditions is obtained and discussed. These include variations of speed, voltage, load and switching angle. The static test characteristics of the motor are carefully measured and the measured flux-linkage data are then used to predict the steady-state performance.

Key Words Switched Reluctance Motor, Dynamic Performance, Performance Prediction Techniques

چکیده برای به‌دست آوردن عملکرد دینامیک ماندگار با زمان محاسباتی کوتاهتر، مدل ریاضی موجود بهبود یافته و ارائه شده است. به کمک این مدل بهبود یافته عملکرد یک نمونه موتور SR تحت محدوده گسترده‌ای از تغییرات شرایط کار به‌دست آمده و مورد بحث قرار گرفته است. این تغییرات عبارتند از تغییر سرعت، ولتاژ، بار و زاویه کلیدزنی. مشخصه‌های آزمایش استاتیک موتور به دقت اندازه‌گیری شده و سپس داده‌های فلوی اندازه‌گیری شده برای پیش‌بینی عملکرد ماندگار ماشین بکار رفته است.

1. INTRODUCTION

Brushless variable speed drives using switched reluctance motors (SRM) have several advantages. The main advantage is the simple structure of the motor with concentrated coils on the stator and no windings or brushes on the rotor [1,2]. In addition, the SRM can operate during the internal and external fault conditions due to the converter unidirectional current requirement [3,4]. Simplified converter circuits can be used [5], since unipolar current is all that is required.

Generally all modelling techniques of SRMs for prediction of steady-state performance are based on the magnetization chracteristics of the motors where different modelling methods differ in handling these data. The nonlinear magnetization characteristics of SRM can be easily modeled analytically by piecewise first or second-order functions of flux-linkage against rotor position, with current as an undetermined

parameter [6]. Although this is an efficient method when average torque is required, it cannot accurately predict the instantaneous torque and current. A more accurate analytical method is due to Pickup and Tipping [7,8], in which they have used a nonlinear equation for flux-linkage curve. Two polynomials, the first for linear and the second for highly saturated regions, can improve the accuracy of the predicted values [9]. Both methods require a large amount of data.

An alternative exponential function has been used for flux-linkage data [10] which is simpler and faster than that given in [7 , 8]. As noted in [11], Stephenson and Corda method (SCM) is a numerical technique to predict the steady-state performance of SRM [12] which has advantages in comparison with the other available analytical methods. The accuracy and short computation time are two major advantages of the method. In order to obtain more accurate predicted steady-state performance with even shorter computation time, the Stephenson and Corda model is modified and used to predict the performance of a 6/4 SRM under a wide range of variations of operating conditions. These include variations of speed, voltage, load and switching angle.

Although several performance prediction methods exist for the SRM, the question does not appear to have been seriously addressed regarding the influence of the variations of speed, voltage, load and switching angle upon the actual dynamic steady-state performance of the SRM. This paper makes a contribution to these ends and presents a modified SCM.

2. THE MOTOR AND SUPPLY

A single tooth per stator pole SRM is proposed in this study. It is the 6-pole, three-phase 6/4 slotted motor with 6 teeth on the stator and 4 teeth on the rotor (henceforth termed the 6/4 motor), constructed in a standard TEFV D100 metric frame. It has the lamination profile shown in Fig. 1.

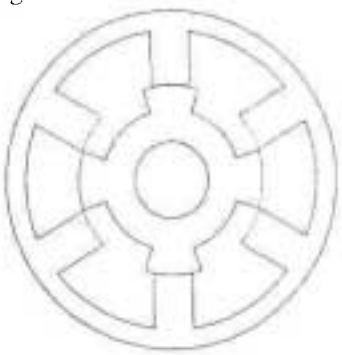

Figure 1. Lamination profile of 6/4 SRM.

The motor phases were switched in turn to rectifier bridge (Figure 2). Excitation of phases is controlled by a rotor position sensor; each phase is excited near the minimum inductance position. Near the maximum inductance position, the phase currents are forced to zero (to reduce retarding torque) by reverse biasing.

3. A MODIFIED PERFORMANCE PREDICTION METHOD

The proposed mathematical model for SRM [12] requires the flux-linkage/current/rotor-angular-positions data. The measured flux-linkage/ current/ rotor - angular - position are represented in Figure 3.

To model the steady-state performance of the SRMs the experimental flux-linkage/rotor-angular-position/current characteristics are required. In order to obtain the experimental data, static test has been performed. In this test, the angle through which the shaft is turned is measured by a displacement transducer mounted on the motor shaft extension. To measure the torque directly, a suitable torque

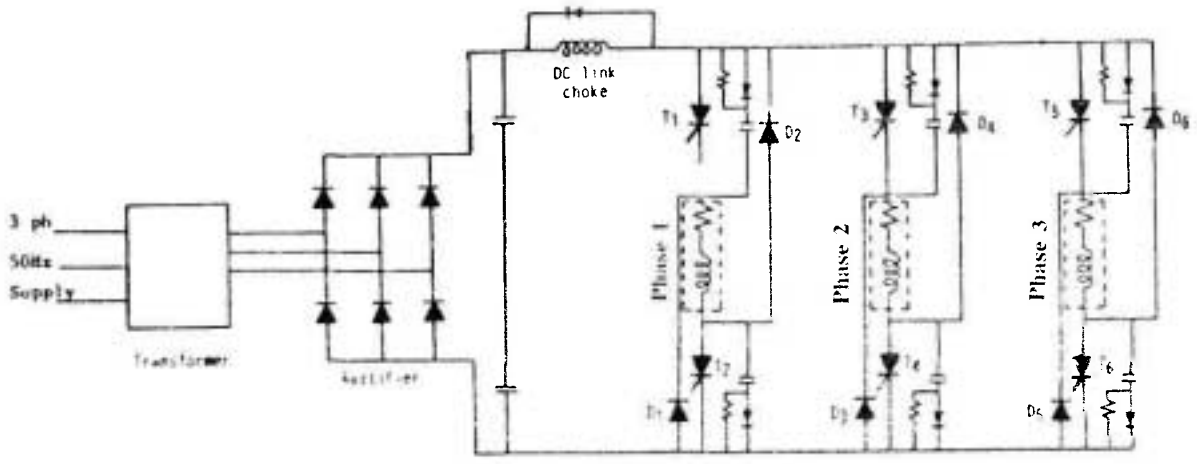

Figure 2. Power circuit for the 6/4 SRM.

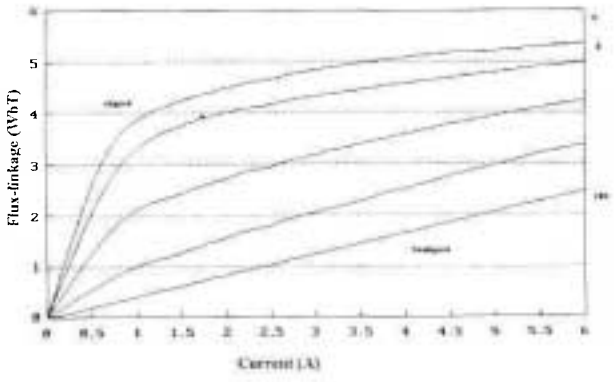

Figure 3. Measured flux-linkage versus rotor current at different rotor angular positions.

transducer is coupled to the motor shaft. A highly stable electronic integrating has measured coil flux-linkage accurately. The torque and flux variation with rotor angular position can be plotted with the desired degree of accuracy by the use of a precision X-Y recorder, and computer digitized for later manipulation. A series of precise dc excitation currents from 0.5 to 6 A are passed into the winding to produce the static characteristics of the motor. The experimental values were digitized to obtain tabulated values of the

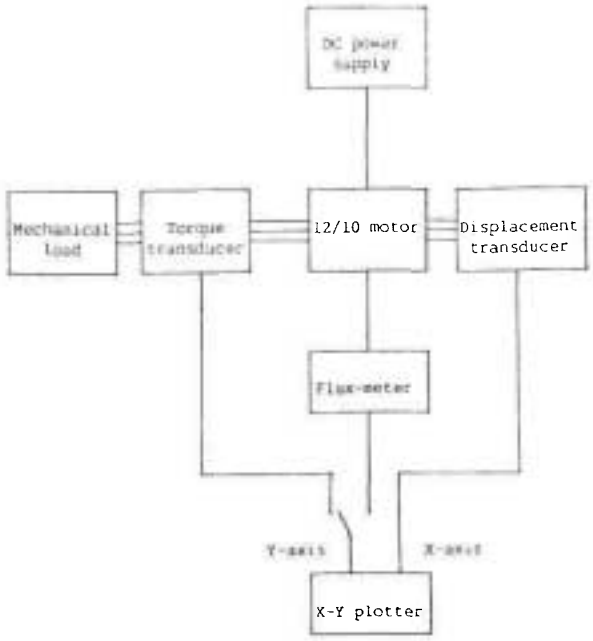

Figure 4. Block diagram of the static test rig.

flux-linkage and static torque versus rotor angular position which are stored on the digital computer for later analysis [13]. The test rig is shown in block diagram representation in Figure 4.

Due to measurement errors the weighted least-squares (WLS) method is used to smooth the flux-linkage characteristics. A quadratic

equation is fitted to the magnetization curve as given below:

$$i(\theta,\Psi) = A\Psi^2 + B\Psi + C \quad (1)$$

where ψ is the flux-linkage. This curve is used for interpolating and generating more points from the measured flux-linkage data. Eq. 1 can also be used for co-energy evaluation:

$$W' = \int_0^{I_0} \psi(\theta, i)di \quad (2)$$

which may also be evaluated as follows:

$$W' = \Psi_0 i_0 - \int_0^{\Psi_0} id\Psi \quad (3)$$

substituting Eq. 1. into Eq. 3 yields:

$$W' = \Psi_0 i_0 - (A\Psi_0^3/3 + B\Psi_0^2/2 + C\Psi_0) \quad (4)$$

Coefficients A, B and C are easily calculated by points α , β , γ , (see Figure 5), their values are constant at each fitting of the quadratic polynomial. Therefore, W′ is evaluated by subtracting the second term of Eq. 4 from the area $i_0\Psi_0$. This procedure is followed for all measured data and a family of co-energy curves is obtained and shown in Figure 6. The motor torque can be calculated from the slope of the above curves as shown below:

$$T(\theta,i) = \frac{\partial}{\partial\theta}\int i\,\psi(\theta,i)di \Big|_{\theta=const} = \frac{\partial W'(\theta,i)}{d\theta}\Big|_{i=const} \quad (5)$$

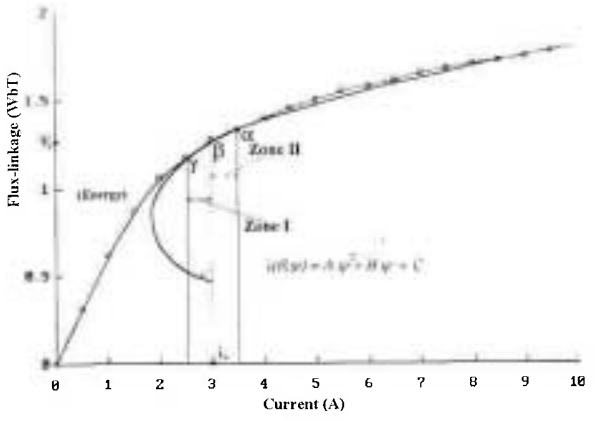

Figure 5. Fitting a quadratic equation to the flux-linkage curve.

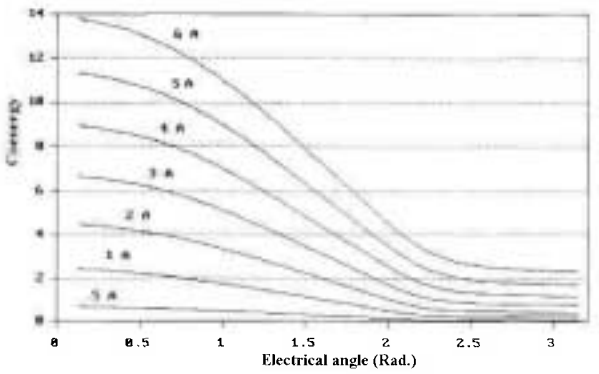

Figure 6. Co-energy curve for the 6/4 SRM.

Note that since the measured angle is in electrical degrees, calculated torque must be multiplied by the number of rotor teeth.

In order to smooth the output results, the Stirling derivative method has been used [12], in which two upper and two lower points around the proposed point have been selected. Then by the help of a difference table and an approximate Stirling equation the derivative is evaluated. It means that in SCM co-energy and torque are calculated numerically which requires a longer computation time. If only one point upper and one point lower than the proposed point are considered and a quadratic equation $W' = D\theta^2 + E\theta + F$ is fitted to these points, then $\delta W'/\delta\theta$ can be easily calculated as follows:

$$\partial W'/\partial\theta = 2D\theta + E \quad (6)$$

Torque can be then calculated using Eq. 6 at different angles. The results obtained by applying the modified method to the 6/4 motor are shown in Figure 7, which show the agreement between the wave forms of the measured and predicted static torque. The analytical method of co-energy and torque evaluation needs a shorter computation time, four times faster than that given in [12], and produces a more accurate result. Also the absolute sum of errors in static torque

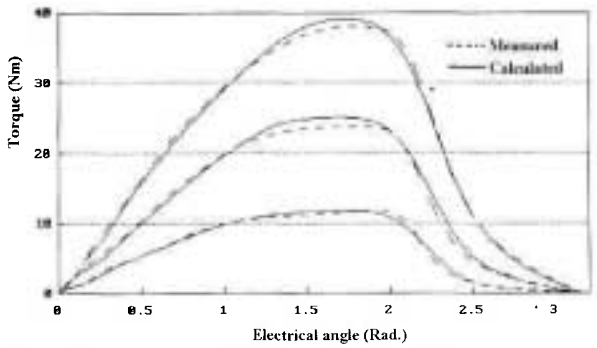

Figure 7. Comparison of computed and measured static torque.

evaluation is 256.9 for SCM and 167.9 for MSCM. A filtering method [14] is used to make a smoother torque curve, which is given for the proposed SRM as follows:

$$T(\theta,i) = \left[1.5\,T(\theta,i-1) + 2T(\theta,i) + T(\theta,i+1) \right] / 4.5 \tag{7}$$

Steady-state performance is evaluated using the following equations:

$$d\Psi(\theta,i)/dt = V - Ri \tag{8}$$

$$d\omega/dt = \left[T(\theta,i) - T_m \right] / J \tag{9}$$

$$d\theta/dt = \omega \tag{10}$$

where T_m is the mechanical torque. The solution of Eqs. 8-10 makes it possible to study the motor behaviour for variations of different performance factors. The flow-chart of the simulation program is presented in Figure 8.

4. INFLUENCE OF SPEED VARIATION

By fixing the amplitude of applied voltage and varying the switching frequency, the motor speed can be adjusted at a required value. To study this in detail, different performance characteristics are considered.

Flux-linkage / current Characteristics Figure 9 shows the trajectories of the operating points on the plane of the phase flux-linkage and the phase current. The areas enclosed by these trajectories are proportional to the developed

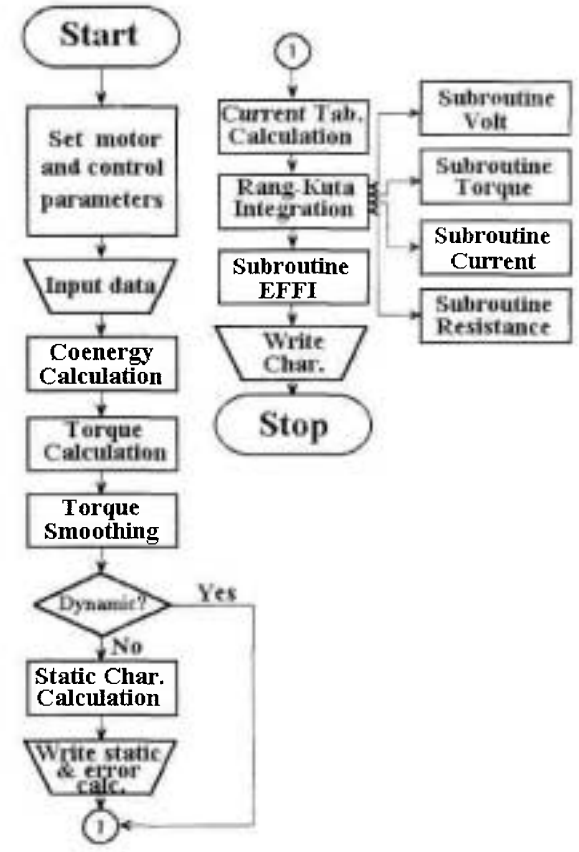

Figure 8. Flow-chart of the developed computer program.

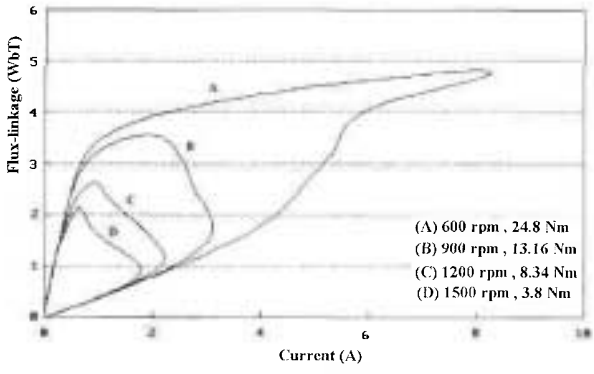

Figure 9. Trajectories of the operating points of the 6/4 SRM on the phase flux-linkage / current plane at different speeds and torques.

torque, being equal to the energy converted ineach step. The trajectories are necessarily bounded by the extreme magnetization curves, which correspond to the aligned and unaligned positions of stator and rotor poles [15]. It will be seen that by increasing the speed up to 1500 rpm (Torque = 3.8 Nm), the enclosed area or converted energy is much lower. It is noted that at a lower speed, such as 600 rpm, more electrical energy can be converted into the mechanical energy. Since the energy is due to one step, increase of frequency, $d\theta/dt$ and ω causes more rapid move of operating point on the trajectory which leads to a smaller enclosed area on the Ψ/i plane and reduction of the mean torque. It is expected that the increase of the speed which in turn would lead to the improvement of the mean torque, current, and the motor performance.

Flux, Current and Torque versus Time Figure 10 denote that by increasing the speed, the amount of flux, current and torque are reduced respectively. In addition more ripples appear on the current and torque wave forms at lower speeds.

Torque, Peak Current, Efficiency and Power Factor Since voltages and currents for SRMs are not normally sinusoidal, the concept of power factor as used with conventional motors has no meaning. Lawrenson et al. [1] have suggested using the concept of 'energy ratio' to measure the quality of power transfer in SRMs. This is the ratio between the useful power and the total power supplied to the motor in one complete cycle of excitation. Harris et al. [16] have shown that this 'energy ratio' does not represent a true measure of the quality of power transfer. The term 'power factor' is used here, for convenience, to express the ratio between the input power and the input

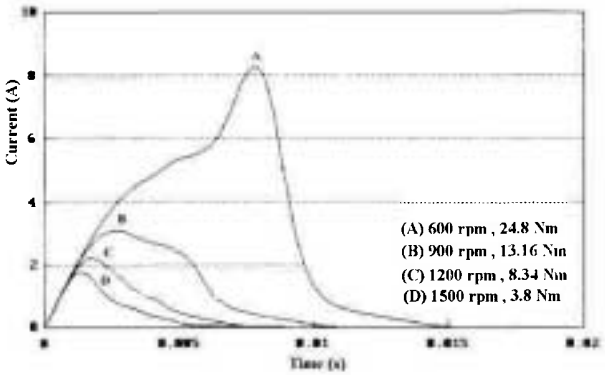

(a)

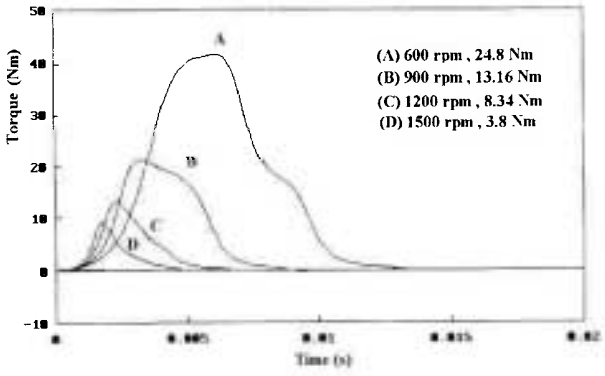

(c)

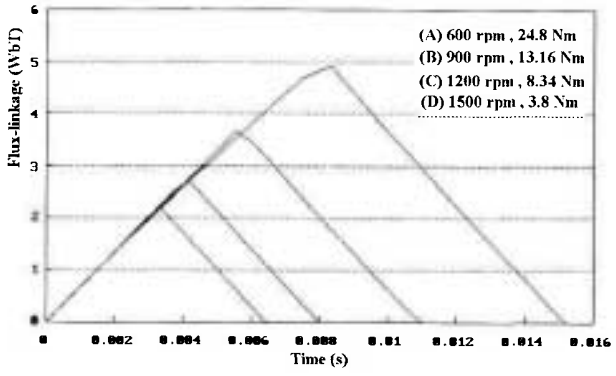

(b)

Figure 10. (a) Current, (b) flux and (c) torque versus time characteristics of the 6/4 SRM at different speeds and torques.

volt-amperes. This ratio is quite low for an SRM. Efficiency has been calculated by referring to the experimental core loss data [17], friction data and evaluated copper losses.

Figure 11 shows mean torque, peak current, efficiency and power factor versus speed between 600 and 1500 rpm for the proposed SRM at two voltages: 282 and 500 V. Referring to Figure 11, at speed 600 rpm, the average torque is maximum and peak current has a larger value. Efficiency and power factors are also high. At speed equal to 1500 rpm, reduction of average torque, efficiency, power factor and peak current is clear. Figure 11b indicates that when the applied voltage is 500 V, only 10% of the efficiency reduction occurs when the speed of motor increases from 600 rpm to 1500 rpm. The corresponding efficiency reduction, when the applied voltage is 282 V, is 33%.

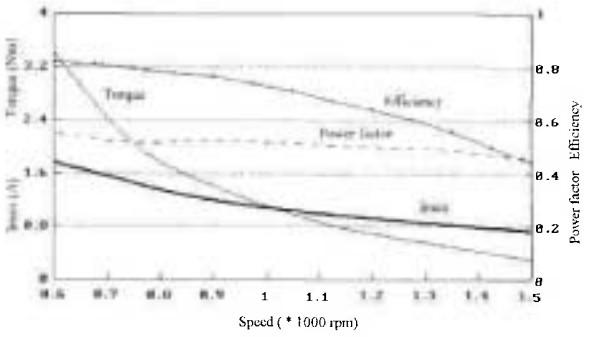

(a)

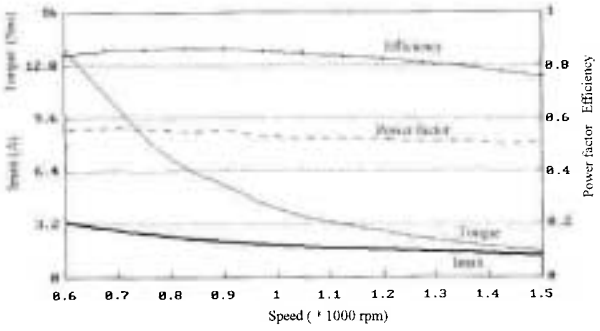

(b)

Figure 11. Torque, peak current, efficiency and power factor versus speed characteristics of the 6/4 SRM: (a) 282 V, (b) 500 V.

5. INFLUENCE OF VOLTAGE VARIATION

By fixing the switching frequency and varying the amplitude of the applied voltage of the SRM, its performance variations with voltage may be determined.

Flux-linkage Versus Current Characteristics Figure 12 shows the flux-linkage current trajectories for the 6/4 SRM, for the speed equal to 1400 rpm. It will be seen that for the higher applied voltage on the SRM (827.3 V at Torque = 12.3 Nm), the enclosed area is much larger. A higher applied voltage means saturated operating region and a higher developed mean torque. However, to limit the core losses in such a saturated region of operation, a thinner ferromagnetic lamination is required to manufacture the motor.

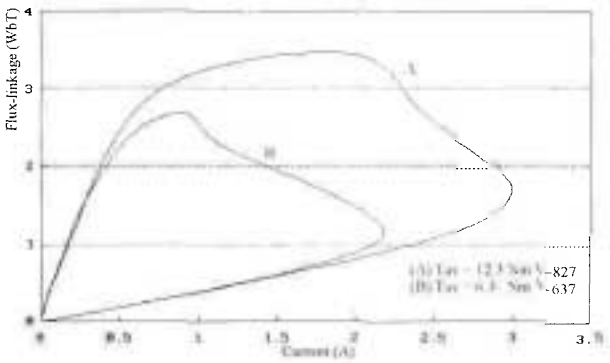

Figure 12. Trajectories of the operating points of the 6/4 SRM on the flux-linkage current plane at different voltages and torques with no chopping control at 1400 rpm.

Flux, Current and Torque versus time Figure 13 reveals that by increasing the applied voltage at the fixed speed equal to 1400 rpm, fewer ripples appear on the current and torque waveforms. Flux, current and torque also rise.

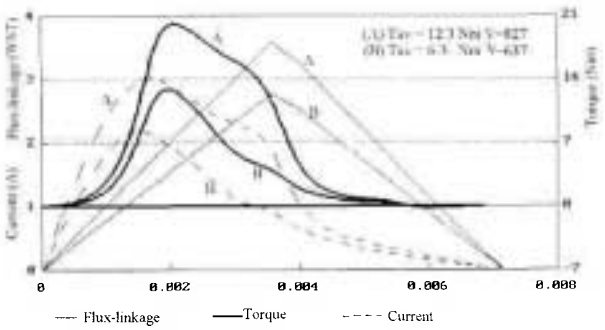

Figure 13. Torque, flux-linkage and current versus time characteristics for the 6/4 SRM at different mean torques and rms voltages for speed 1400 rpm.

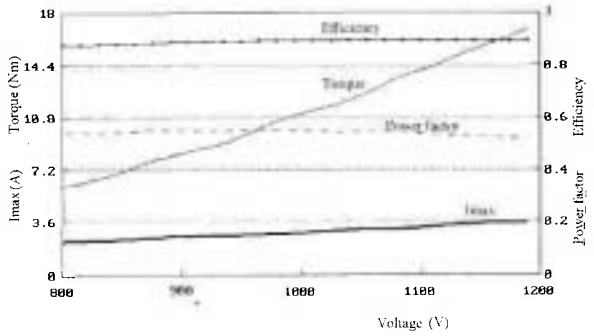

Figure 14. Torque, peak current, efficiency and power factor versus voltage characteristics of the 6/4 SRM at 1400 rpm.

Torque, Peak current, Efficiency and Power Factor Figure 14 indicates that lower torque and peak current occur at lower voltage equal to 800 V. the opposite is true for the higher voltage equal to 1200 V. Efficiency is slightly lower for the higher voltage.

When the applied voltage is varied, the average torque varies linearly with the voltage, and change of frequency can only displace the location of the peak torque; therefore, adjusting the stable region of the motor is possible.

6. INFLUENCE OF LOAD VARIATION

SRM can be simulated for different loads by fixing applied voltage and frequency of the motor. Variation of average torque, instantaneous torque, flux, instantaneous current, average torque to rms current, peak current, efficiency and power factor are studied for this case.

Flux-linkage versus Current Characteristics As Figure 15 shows by reducing the motor load, the enclosed area on the flux-linkage-current curve is decreased which leads to a lower average torque of the motor.

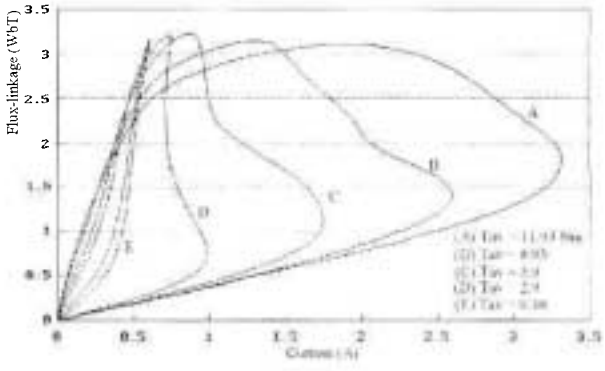

Figure 15. Trajectories of the operating points of the 6/4 SRM on the flux-linkage plane.

Flux, Current and Torque versus time Reduction of the load decreases the instantaneous current (Figure 16a). Also this load reduction diminishes the cutoff angle θ_2 (aligned position) to zero which produces a negative torque and the total torque reaches zero (Figure 16b). Of course instantaneous flux does not change and is almost constant (Figure 16c).

Torque, Peak Current, Efficiency and Power Factor The results show that motor performance is improved by increasing the load, because efficiency, power factor and mean torque/phase current ratio become larger (Figure 17). In this case, the peak current will be also higher in order to develop more torque.

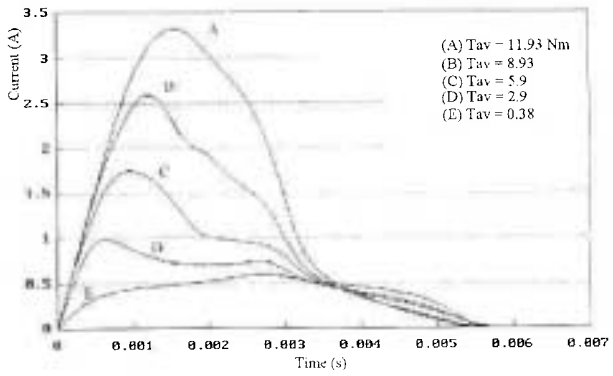

(a)

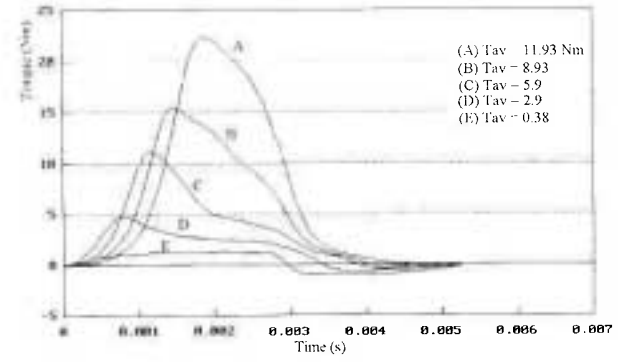

(b)

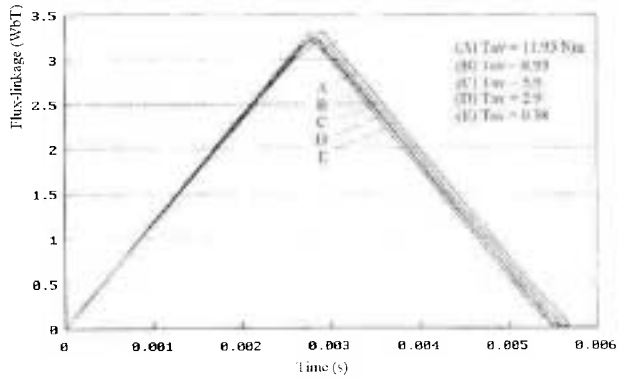

(c)

Figure 16. Instantaneous (a) current, (b) torque and (c) flux-linkage for the 6/4 SRM at different torques and speed of 1000 rpm.

7. INFLUENCE OF SWITCHING ANGLE VARIATION

Different angles are defined in Figure 19 with reference to the inductance profile of one phase. θ_1 , θ_2 and θ_D are turn-on angle, turn-off angle and dwell angle respectively.

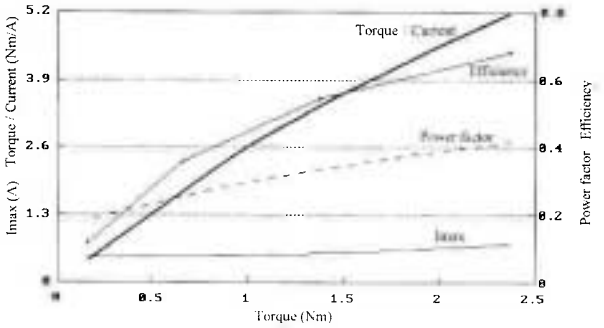

Figure 17. T/I, peak current, efficiency and power factor versus torque curves for the 6/4 SRM at 900 rpm and 720V.

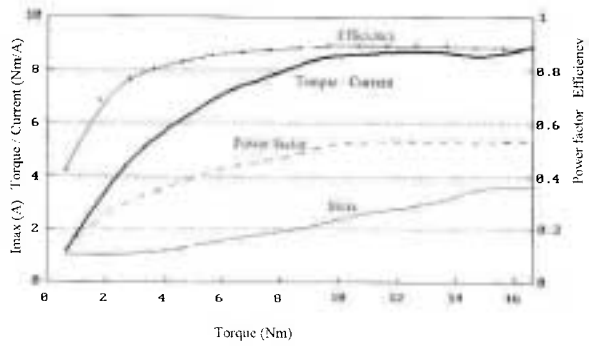

Figure 18. T/I, peak current, efficiency and power factor versus torque curves for the 6/4 SRM at 1500 rpm and 1200 V.

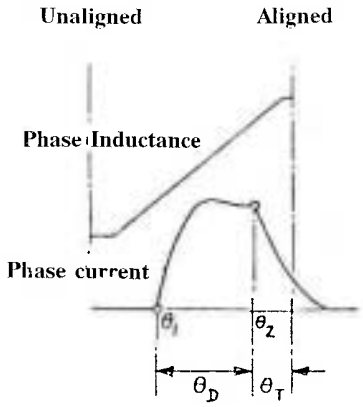

Figure 19. Definition of angles θ_1 , θ_2 and θ_D.

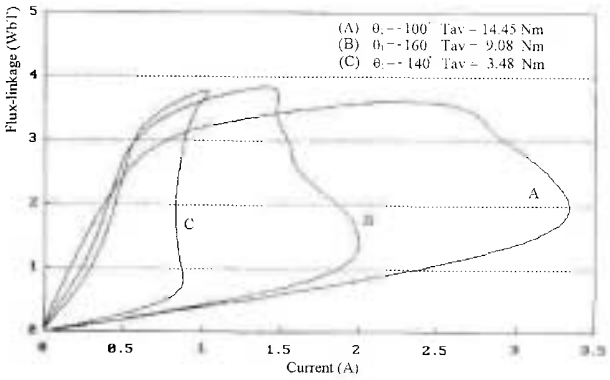

Figure 20. Trajectories of the operating points of the 6/4 SRM on the flux-linkage/current plane at different torques and angles θ_1 at $\theta_2 = -60$ degrees.

Flux-linkage versus current characteristics By fixing θ_2 and varying θ_1 , performance of SRM can be controlled. Figure 20 shows that the SRM is quickly saturated by increase of angle θ_1. The enclosed area on the flux-linkage current trajectories become lower and developed mean torque becomes smaller.

Flux, Current and Torque versus time Figure 21 indicates that by increasing θ_1 , there is no time to increase the motor current; therefore, torque, current and flux reduce and less power is delivered to the load. Since each phase has less contribution to the development of torque and consuming current, the torque and current contain more ripples.

Flux-linkage versus current characteristics By fixing θ_1 and varying θ_2 , performance of SRM can be controlled. Figure 22 shows that the SRM current diminishes quickly by decrease of angle θ_2 . There is no time to increase the enclosed area on the flux-linkage-current trajectory and, therefore, the developed mean torque is lower.

Flux, Current and Torque versus time Figure 23 indicates that flux, current and torque diminish quickly and the ripples of the current

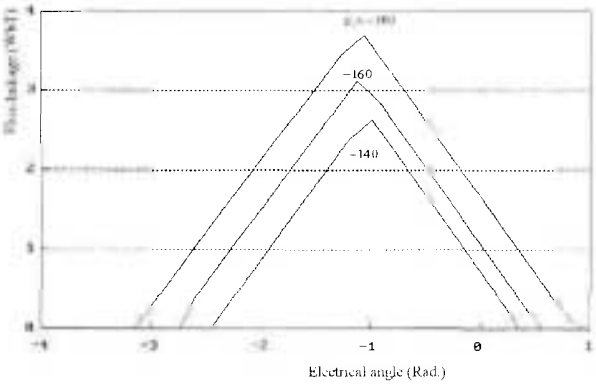

(a)

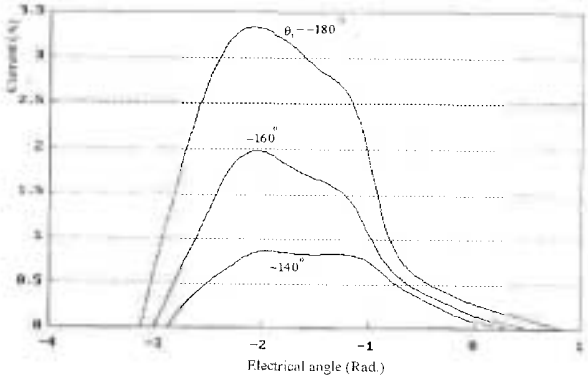

(b)

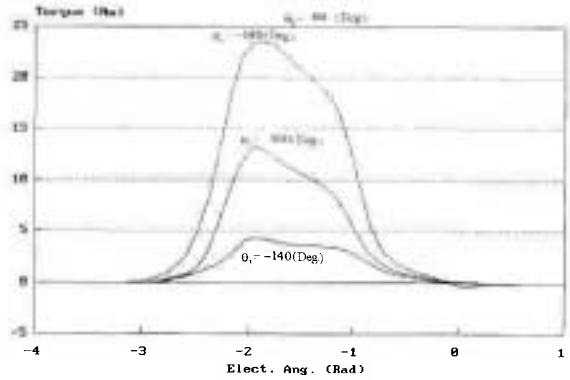

(c)

Figure 21. Instantaneous (a) flux-linkage, (b) current and (c) torque for the 6/4 SRM with different angles θ_1 at $\theta_2 = -60$ degrees.

waveform become higher by decreasing θ_2 . While by reducing θ_2 initially mean torque increases (because of reduction of negative torque), when it approaches the maximum

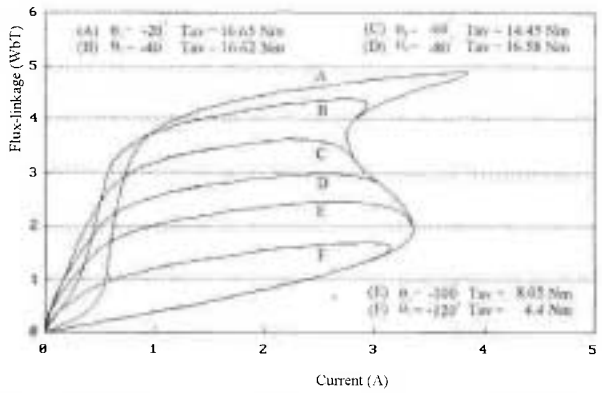

Figure 22. Flux-linkage/current trajectories for the 6/4 SRM with different θ_2 angles at $\theta_1 = -100$ degrees.

torque, the mean torque decreases.

Variation of θ_D By simultaneous varying of θ_1 and θ_2 in such a way that the switching band remains constant, SRM can be controlled. For a similar investigation in [19] peak current power factors are neglected which are considered here in motor performance prediction.

Torque variation with θ_D The operating region of the motor can be divided into two parts (Figure 24). The right hand side of the maximum torque is the stable region and the left hand side of the maximum torque is the instable region. By increasing θ_D , the maximum torque rises and its location on the plane also moves. This move is about 10 electrical degrees which may be ignored. By preventing the motor to reach the maximum torque, SRM can be controlled as reported in [19].

Peak current variations In the stable region, the peak current is reduced by the reduction of θ_2 , also by the reduction of the motor efficiency, peak current increases which provides the suitable operating conditions. Therefore, it is necessary to adjust angle θ_2 at a possible minimum value.

Efficiency Variations Similar to torque curve,

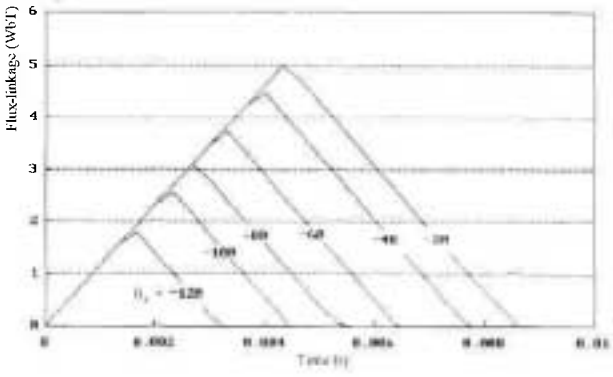

(a)

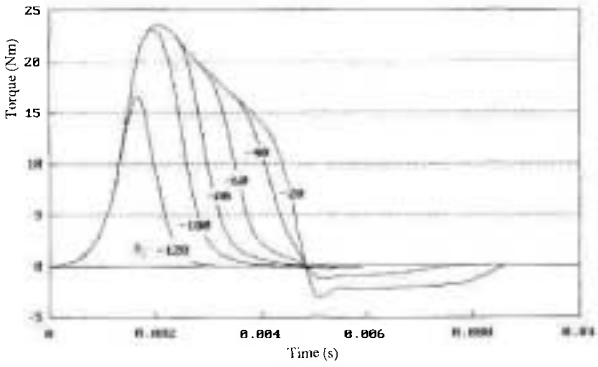

(b)

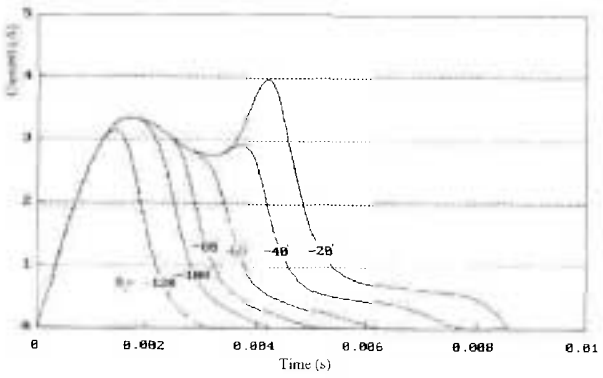

(c)

Figure 23. Instantaneous (a) torque, (b) current and (c) flux linkage for the 6/4 SRM with different θ_2 at θ_1=-100 degrees.

efficiency is maximized around the maximum torque. This is located in the stable region. Therefore, by increasing θ_D , the motor can be stabilized and also have maximum efficiency.

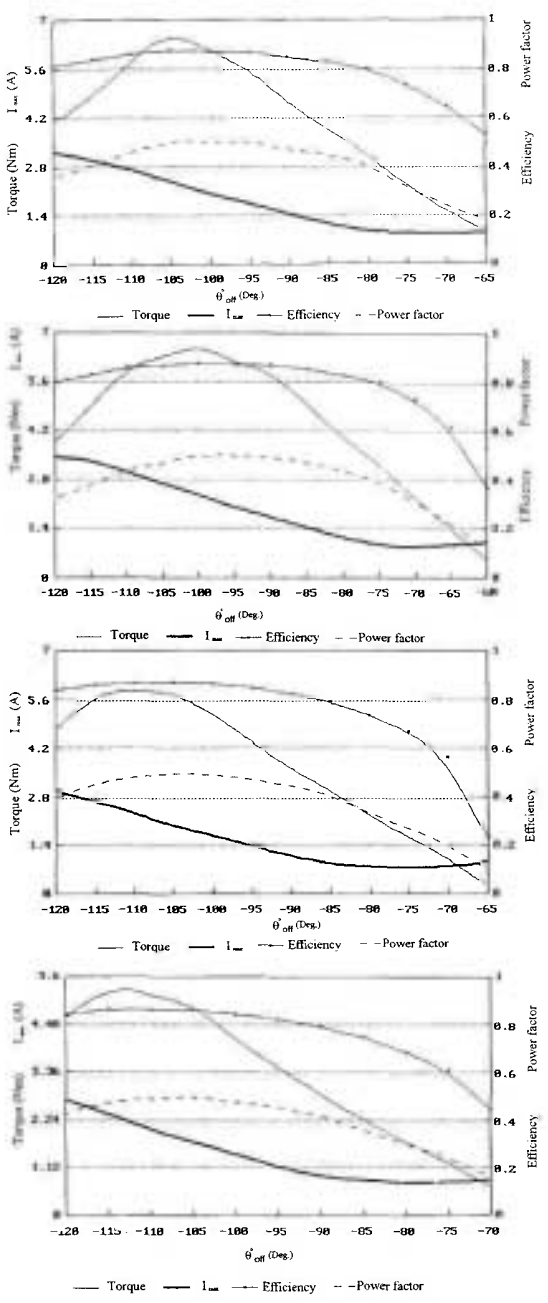

Figure 24. Torque, peak current, efficiency and power factor variations with θ_2 at $\theta_D = 65$, $\theta_D = 60$ $\theta_D = 55$ and $\theta_D = 50$ degrees.

However, a compromise between the increase of stabilization and optimum efficiency must be made.

Power Factor Variations Variation of θ_D has almost no effect on the power factor. Therefore, there is no possibility to control and improve the power factor except when θ_D is reduced. In such a case, stability of the SRM may be lost.

Study of the results show that control of the switching angle is a very effective factor in controlling the SRM performance. Varying voltage and switching frequency have some limits and need rotor position sensors, but control of the switching angles has no such limitations.

8. CONCLUSIONS

A modified Stephenson and Corda method (MSCM) has been presented for predicting the steady-state performance of the 6/4 SRM. It was shown that this model is 4 times faster than the SCM and it achieves better accuracy compared with the SCM. The dynamic steady-state performance variation of the SRM against variation of speed, applied voltage, switching angles and load have been studied. It was noted that the control of maximum current of SRM must be considered for effective control of the motor.

ACKNOWLEDGMENT

We would like to acknowledge University of Tabriz for the project financial support.

REFERENCES

1. P. J. Lawrenson, et al., "Variable Speed Switched Reluctance Motors", ***Proc. IEE,*** Pt. B, Vol. 127, No. 4, (July 1980), 253-265.
2. P. N. Materu and R. Krishnan, "Steady-state Analysis of the Variable Speed Switched Reluctance Motor", ***IEEE Trans. on Industrial Electronics***, Vol. 36, (Nov.

1989), 523-529.

3. H. Le-Huy, P. Viarogue and P. Francocur, "Unipolar Converters for Switched Reluctance Motors", In Rec. (1989), ***IEEE Industry Applications Soc. Ann. Meeting***, 551-560.
4. J. T. Bass, et al., "Development of Unipolar Converter for Variable Reluctance Motor Drives", ***IEEE Trans. on Industry Applications***, Vol. IA-23, (May/June 1987), 545-553.
5. W. F. Ray and R.M. Davis, "Inverter Drive for Doubly-Salient Reluctance Motor, its Fundamental Behavior, Linear Analysis and Cost Implication", ***Proc. IEE***, Pt. B. No. 6, 185-193.
6. Ilic-Spong et al., "Nonlinear torque control of electric motor drives-part II", ***PESC Record***, (1986), 456-475.
7. I. E. D. Pickup and D. Tipping, "Method for Predicting the Dynamic Response of a Variable Reluctance Stepping Motor", ***Proc. IEE***, Vol. 120, No. 7, (July 1973), 757-764.
8. I. E. D. Pickup and D. Tipping, "Prediction of Pull-out Rate and Settling Time Characteristics of a Variable Reluctance Stepping Motor and Effect of Stator Damping Coils on these Characteristics, ***Proc. IEE***, Vol. 123, No. 3, (March 1976), 213-219.
9. J. W. Finch, H. M. B. Metwally, "Performance Prediction of Saturated Variable Reluctance and Hybrid Motors", ***International Conference of Power Electronics and Variable Speed Drives***, London, (September 1989), 231-236.
10. D. A. Torrey, J. N. Lang, "Modeling a nonlinear Variable-Reluctance Motro Drive", ***IEE Proc.***, Vol. 137, Pt. B, No. 5, (September 1990), 314-326.
11. J. Faiz, "A Review of the Performance Prediction and Design Techniques for Switched Reluctance Motors", ***Journal of Electrical and Electronics Engineering***, Australia, Vol. 12, No. 3, (September 1992), 258-266.
12. J. Corda and J.M. Stephenson, "Computation of Torque and Current in Doubly-Salient Reluctance Motors from Nonlinear Magnetization Data", ***Proc. IEE***, Vol. 126, (May 1979), 393-396.
13. J. Faiz, J. W. Finch and H. M. B. Metwally, "A Novel Switched Reluctance Motor with Multiple Teeth Per stator Pole and Comparison of such Motors", ***International Journal of Electric Power Systems Research***, Vol. 34, (1995), Elsevier, 197-203.
14. S. Haykin, "Adaptive Filter Theory", Printice Hall, London, (1991).
15. M.R. Harris, et al., "A Review of the Integral-Horsepower Switched Reluctance Drive", ***IEEE Trans. on Industry Applications***, Vol. IA-22, No. 4, (July/August 1986), 716-721.
16. M.R. Harris et al., "Discussion on Variable- Speed Switched Reluctance Motor Systems", ***IEE Proc. Pt. B***, 128, (1981), 260-268.
17. H. M. B. Metwally, J. Faiz and J. W. Finch, "Core loss in Switched Reluctance Motor Structure-Experimental Results", ***Proc. of International Conference of Electrical Machines (ICEM-88)***, (Sept. 1988), Pisa, Italy, Vol. II, 31-34.
18. J. R. French, "Switched Reluctance Motor Drives for Rail Traction, Relative Assessment", ***IEE Proc.***, Part B, Vol. 131, NO. 5, (September 1984), 209-219.
19. T. J. E. Miller, J. T. Bass and M. Ehsani, " Stabilization of VRMD Operating Without Shaft Position Feedback", ***14th Symposium Incr. Motion Control System & Devices***, University of Illinois, (1985), 361-367.